Inverter Device Nonlinearity Characterization Technique for Use in a Motor Drive System

Andrew S. Babel, *Student Member, IEEE*, Annette Muetze, *Senior Member, IEEE*, Roland R. Seebacher, Klaus Krischan, and Elias G. Strangas, *Member, IEEE*

***Abstract*—This paper introduces a detailed nonlinearity characterization technique for insulated-gate bipolar transistor inverters in a drive system which is able to measure device nonlinearities. Methods are derived from measurements of the voltage on the inverter phases. These measurements are obtained while applying a set of direct currents to an electrical machine. These methods are then applied to tests using alternating current. The study of inverter nonlinearities is useful in order to conduct condition monitoring. These methods fulfill the need to characterize each device in an inverter. In addition to characterizing every device using either ac or dc current, the method is resistant to noise; for these reasons, the method is applicable in the field. Simulations and experimental work demonstrate the benefits and applicability of the methods.**

***Index Terms*—Condition monitoring, insulated-gate bipolar transistors, inverter characterization, power semiconductor devices, three-phase electric power.**

NOMENCLATURE

DFT	Discrete Fourier transform.
FFT	Fast Fourier transform.
STFT	Short-time Fourier transform.
B	Frequency width of STFT window.
D	Duty cycle.
C_k	Fourier coefficients at k.
f_{c}	Carrier frequency.
f_1	Fundamental power frequency.
h	Window function.
i_{X}	Current in phase X.
J_{m}	mth-order Bessel function of the first kind.
M	Modulation index.
N	Samples per period of the pulse width modulation (PWM) signal.
N_{p}	Positive samples per period of the PWM signal.
s	Signal which the STFT is performed on.
T	Time width of STFT window.
T_{c}	Carrier period.
$V^{\mathrm{AC}}_{\mathrm{X\to DCN}}$	Voltage measured from phase X to the negative dc link with alternating load current.
$V^{\mathrm{DC+/-}}_{\mathrm{X\to DCN}}$	Voltage measured from phase X to the negative dc link with positive or negative direct load current.
V_{sdrop}	Semiconductor voltage drop.
x	Analytic representation of PWM signal.
$\hat{x}$	Frequency spectrum of x.
μ_{x}	Mean of the signal x.

Manuscript received May 28, 2014; revised August 18, 2014; accepted October 3, 2014. Date of publication October 29, 2014; date of current version May 15, 2015. Paper 2014-IPCC-0410.R1, presented at the 2014 IEEE Applied Power Electronics Conference and Exposition, Fort Worth, TX, USA, March 16–20, and approved for publication in the IEEE TRANSACTIONS ON INDUSTRY APPLICATIONS by the Industrial Power Converter Committee of the IEEE Industry Applications Society. This paper is based upon work supported by the Marshall Plan Foundation Scholarship and the National Science Foundation under Grant 1102316. Additional funding was provided by the Michigan State University Graduate Student Research Enhancement Award.

A. S. Babel and E. G. Strangas are with the Department of Electrical and Computer Engineering, Michigan State University, East Lansing, MI 48824-1226 USA (e-mail: babeland@msu.edu; strangas@egr.msu.edu).

A. Muetze, R. R. Seebacher, and K. Krischan are with the Electric Drives and Machines Institute, Graz University of Technology, 8010 Graz, Austria (e-mail: muetze@tugraz.at; roland.seebacher@tugraz.at; klaus.krischan@tugraz.at).

Color versions of one or more of the figures in this paper are available online at http://ieeexplore.ieee.org.

Digital Object Identifier 10.1109/TIA.2014.2365636

I. INTRODUCTION

SEMICONDUCTOR devices have a nonlinear anode–cathode or collector–emitter voltage drop with respect to the diode current or collector current, respectively. The aim of this work is to develop a technique to find the voltage–current characteristic of each of the insulated gate bipolar transistors (IGBTs) and diodes constituting a typical industrial inverter. The forward voltage drop is the only practically measurable quantity, given the typical industrial drive sensor setup of current and voltage sensors on the phases; it is not possible to extract the gate-to-emitter voltage, another voltage drop in an IGBT, because there are no voltage sensors connected to the gate. The turn-on and turnoff times of the semiconductors are not measured because this paper studies only the static device voltage drop characteristics.

Typically, the nonlinear inverter voltage drops are ignored, or the effects of the drops are removed by the controller (e.g., [1]–[9]). Knowledge of the inverter nonlinearity values is important for three applications: voltage distortion, sensorless control, and condition monitoring.

The works in [1]–[4] develop methods to remove the effects of the inverter voltage drop from the output voltage. The removal of these nonlinearities results in an output with less error with respect to the commanded voltage; accurate voltage is especially important while operating at a low speed or with low current.

The performance of sensorless drive schemes is improved in [4]–[9] using knowledge of the inverter nonlinearities. Sensorless drive schemes often use a flux observer, a position observer, or some combination of the two. Observers typically use the machine model, but without a nonlinear inverter model, the performance of observers degrades, with an error between the commanded and the attained voltage. Therefore, adding such an inverter model can improve performance.

Condition monitoring for inverters is nascent but has been discussed in some work, such as [10]–[12]. The magnitude of the voltage drop can also reflect the health of each of the devices. Condition monitoring applied to inverters investigates the value of these nonlinearities; a change in these can indicate a developing fault.

The data sheet parameters generally suffice for compensation purposes, as at least the linear approximation is given. Characterization is only useful if the parameters change during operation whether due to bonds lifting or other causes. While characterization may be useful for improving the voltage compensation scheme if the parameters change, the primary motivation of this paper is condition monitoring.

In the work by Yang *et al.* [10], physics-based reliability models are given for inverter semiconductor faults. Because of the prevalence of bond wire lift-off (BWLO) faults, they are the motivation for this work.

Other works, such as [13]–[18], investigate the diagnosis of BWLO faults. There are two main tools for diagnosing these faults: The first is by detecting a fault with voltage or current harmonics, as well as other current signatures, or other test equipment, and the second is by using device parameter information.

The first diagnostic approach using harmonics is commonly taken for detecting faults in a variety of applications. In [13], Diallo *et al.* use the current space vector trajectory to determine if the IGBTs are all operating normally. In [16], an external circuit is added to the inverter to monitor the switching transitions—this is used to detect improper switching caused by faulty devices. A similar approach is taken in [16] to detect if an IGBT fails to conduct when the gate signal commands it to. The magnetizing and torque-producing current components in an induction machine are used to diagnose device faults in [17]. The phase voltage harmonics are used to determine if a fault is present in [14].

The diagnosis approach of parameter characterization serves as the motivation for this paper. Xiang *et al.*, in [14], demonstrate that BWLO has an effect on the device parameters, although determining the parameters is difficult. With the introduction of an accurate characterization method, as is introduced in this paper, the parameters can be used for diagnosis purposes.

The authors in [1], [4], [5], and [19] find the average voltage drop of the IGBT and its freewheeling diode; their goal is to remove the effect of the nonlinearity and not condition monitoring. The offline method in [1] uses the voltage command and measured current together with a flux observer that estimates the linearized voltage–current relationship. Liu and Zhu [4] estimate the voltage distortion online using an adaline observer while the machine is operating with no current in the direct axis. The authors of [5] and [19] discuss similar methods which use a machine model and a standstill dc test to find the voltage–current relationship. Both methods operate by measuring the voltage while applying a series of direct currents with different magnitudes to the inverter phase. The result is a voltage–current relationship that is the average of the voltage drop over the IGBT and its corresponding freewheeling diode.

For widespread application in the field, a technique needs to be both simple and able to characterize each device in detail. This paper seeks to characterize an inverter in detail over its entire current operating range. To isolate each individual quantity, new and simple characterization methods have been developed. These new methods use voltage sensors placed between the inverter phases and the negative dc link. The first method, referred to as the "mean method," works with the application of direct currents and the mean of the sensed voltage to solve for both of the two voltages, V_{igbt} and V_{diode}, using the sensed currents, voltages, and applied duty cycle. Multiple current magnitudes are applied in order to get the entire current range of the device. The second method, referred to as the "spectral method," uses the same measured quantities, as well as the voltage harmonic content; this is done by analytically determining the relationship between the Fourier transform components and the device voltages. The spectral method used in the dc case is then extended to the ac case with the STFT [20].

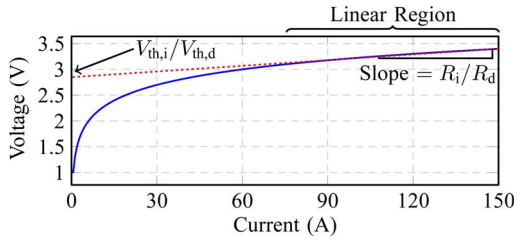

Fig. 1. Waveforms showing a generalized semiconductor nonlinearity, given as its voltage–current characteristics and the linear approximation to this with its equivalent parameters; this is the key characteristic for a device. The inverter used in this work is the 1200-V 250-A SEMIKRON SKiiP 2.

Section II develops the representation of the voltage nonlinearity. Section III introduces novel characterization methods with dc. Section IV extends the dc characterization methods for use with ac.

II. Representing the Semiconductor Voltage Drop

A series of tests is used to determine the entire voltage–current relationship of the device. Current is applied to each of the devices, and the device voltages are determined from measurements.

There are four characteristics which define the nonlinearity: The resistance (R_{d}, differential resistance of linear region) and forward biased junction voltage $(V_{\mathrm{th,d}})$ over the diode, as well as the resistance (R_{i}, differential resistance of linear region) and forward biased junction voltage $(V_{\mathrm{th,i}})$ over the IGBT. These quantities form a linear approximation to the device nonlinearity, as shown in Fig. 1. The linear region begins where the linear approximation and actual characteristic curve are close. This varies by device, but it is assumed to be where the differential resistance becomes less than twice its final value in Fig. 1, at roughly 125 A (the differential resistance decreases with current). This linear approximation is helpful for simplification and to determine the saturation behavior of the device, but the nonlinear area below this is also important to fully characterize the device behavior.

The methods all require that the device voltages be calculated from the phase voltage measurements. With the phase and

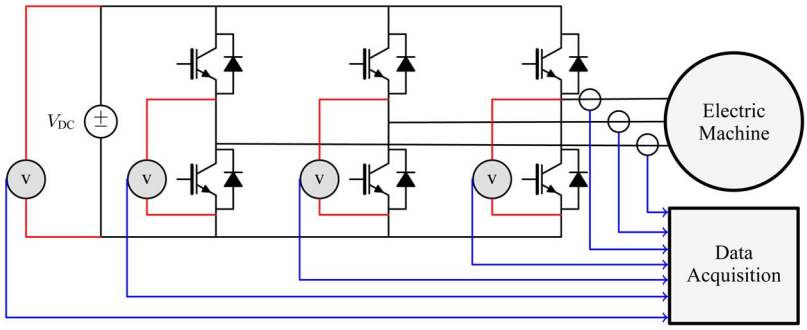

Fig. 2. Experimental setup for inverter characterization is shown with the line-to-DCN voltage sensors.

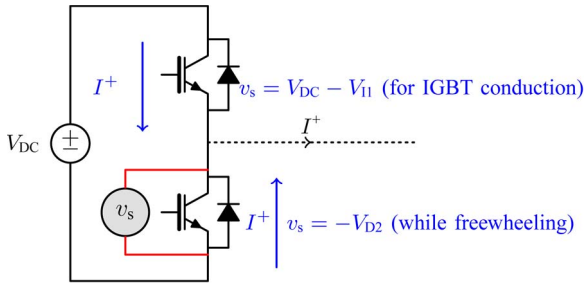

Fig. 3. Phase A half bridge of the inverter, showing the sensor connection. The purpose of this figure is to demonstrate the paths of current and how they relate to the voltage measured by the voltage sensor.

dc link voltage sensors shown in Fig. 2, the information required to characterize the devices is available, as shown in the next paragraph.

A. Analytic Expression for Voltage Drop With Direct Load Current

An analytic expression for the voltage drop with direct load current is derived using the discussed sensor placement. We demonstrate that these sensors are sufficient for characterization using the following situation: Assume that phase A of the inverter conducts a positive current into the load. When the switching command for phase A is high, the top IGBT conducts; when it is low, the bottom diode conducts (freewheels). These two paths are illustrated in Fig. 3. When the bottom diode is conducting during freewheeling, the voltage measured will be the bottom diode voltage with a negative sign. When the IGBT is conducting, the voltage will be that of the dc link less the IGBT voltage drop. The IGBT voltage drop can therefore be calculated using $V_{\mathrm{DC}} - V_{\mathrm{A}\to\mathrm{DCN}}$.

The measured voltage $V_{\mathrm{A}\to\mathrm{DCN}}$ resembles the waveform in Fig. 4(a) for positive current ($V^{\mathrm{DC}+}_{\mathrm{A}\to\mathrm{DCN}}$). The negative current case is given in Fig. 4(b). The effect of the dc link should be removed, as we are only interested in the diode and IGBT voltages. This is only discussed for the positive load current case; the dc-link voltage is removed, and the resulting square wave was made to intersect with 0 V, with the positive and negative values corresponding to the IGBT and diode, respectively. When this square wave is high, the dc-link voltage is subtracted from the value, and the result is negated; when low, nothing is done. The removal of dc-link voltage and negation when high results in the waveform shown in Fig. 4(c). The values

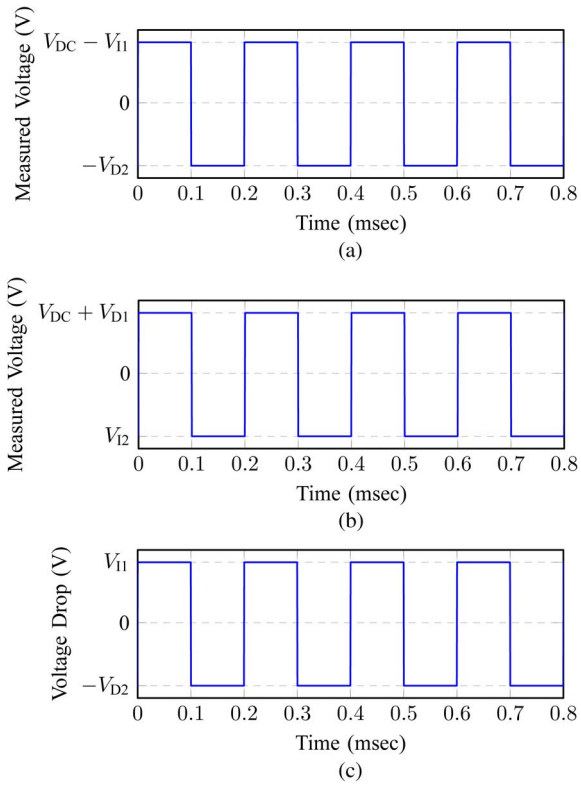

Fig. 4. Representations of the voltages measured with the sensor configuration in Fig. 2. (a) Voltage measured from phase A to the negative dc link, $V^{\mathrm{DC}+}_{\mathrm{A}\to\mathrm{DCN}}$. (b) Voltage measured from phase A to the negative dc link, $V^{\mathrm{DC}-}_{\mathrm{A}\to\mathrm{DCN}}$. (c) Extracted semiconductor device voltage drop representation, $V^{\mathrm{DC}+}_{\mathrm{sdrop}}$, used in analysis.

between the positive and negative maximum areas are ignored. The modified waveform is referred to as the semiconductor voltage drop, V_{sdrop}, and is used for the subsequent analysis. The waveforms for the positive and negative cases will take the following shape: For the positive current case, the square wave positive value should be V_{I1}, and the square wave negative value should be $-V_{\mathrm{D2}}$; for the negative current case, the square wave positive value should be V_{I2}, and the square wave negative value should be $-V_{\mathrm{D1}}$.

The analytic expressions for the measured phase A voltage with positive direct load current, $V^{\mathrm{DC}+}_{\mathrm{A}\to\mathrm{DCN}}$, and measured voltage with negative load current, $V^{\mathrm{DC}-}_{\mathrm{A}\to\mathrm{DCN}}$, are found first. The two expressions are then combined into the complete phase

A measured voltage expression with the applied dc current, $V^{\mathrm{DC}}_{\mathrm{A}\to\mathrm{DCN}}$. In Fig. 4(a), $V^{\mathrm{DC+}}_{\mathrm{A}\to\mathrm{DCN}}$ is plotted; only the voltages for the top IGBT of phase A (IGBT1/I1) and the bottom diode of phase A (diode2/D2) are measurable. The analytic expression for $V^{\mathrm{DC+}}_{\mathrm{A}\to\mathrm{DCN}}$ is given for $0 \le t < T_{\mathrm{c}}$ by (1) as a pulse train waveform with a constant duty cycle. In Fig. 4(b), $V^{\mathrm{DC-}}_{\mathrm{A}\to\mathrm{DCN}}$ is plotted; for this case, the voltages for the bottom IGBT of phase A (IGBT2/I2) and the top diode of phase A (diode1/D1) are measurable. The analytic expression for $V^{\mathrm{DC-}}_{\mathrm{A}\to\mathrm{DCN}}$ is given by (2). Equation (3), $V^{\mathrm{DC}}_{\mathrm{A}\to\mathrm{DCN}}$, is found from $V^{\mathrm{DC+}}_{\mathrm{A}\to\mathrm{DCN}}$ and $V^{\mathrm{DC-}}_{\mathrm{A}\to\mathrm{DCN}}$, where $\mathrm{sgn}\{i_{\mathrm{a}}\}$ represents the direction of the phase A load current

$$V^{\mathrm{DC+}}_{\mathrm{A}\to\mathrm{DCN}}(t) = \left[V_{\mathrm{DC}} - V_{\mathrm{I1}}(i_{\mathrm{a}})\right] u(t) - \left[(V_{\mathrm{DC}} - V_{\mathrm{I1}}(i_{\mathrm{a}})) + V_{\mathrm{D2}}(i_{\mathrm{a}})\right] u(t - DT_{\mathrm{c}}) \tag{1}$$

$$V^{\mathrm{DC-}}_{\mathrm{A}\to\mathrm{DCN}}(t) = \left[V_{\mathrm{DC}} + V_{\mathrm{D1}}(i_{\mathrm{a}})\right] u(t) + \left[V_{\mathrm{I2}}(i_{\mathrm{a}}) - (V_{\mathrm{DC}} + V_{\mathrm{D1}}(i_{\mathrm{a}}))\right] u(t - DT_{\mathrm{c}}) \tag{2}$$

$$V^{\mathrm{DC}}_{\mathrm{A}\to\mathrm{DCN}}(t) = V^{\mathrm{DC+}}_{\mathrm{A}\to\mathrm{DCN}}(t) \left\{\frac{1}{2}\left(\mathrm{sgn}\,(i_{\mathrm{a}}) + 1\right)\right\} + V^{\mathrm{DC-}}_{\mathrm{A}\to\mathrm{DCN}}(t) \left\{\frac{1}{2}\left(1 - \mathrm{sgn}(i_{\mathrm{a}})\right)\right\}. \tag{3}$$

If V_{DC} varies, this has a negative effect on the accuracy of the calculation result. By measuring V_{DC} and removing the effect, (1) and (2) become (4) and (5) (V_{sdrop}). V_{sdrop}, previously discussed, is the voltage drop over the inverter semiconductors; this is the voltage used hereafter

$$V^{\mathrm{DC+}}_{\mathrm{sdrop}}(t) = \left[V_{\mathrm{I1}}(i_{\mathrm{a}})\right] u(t) - \left[V_{\mathrm{I1}}(i_{\mathrm{a}}) + V_{\mathrm{D2}}(i_{\mathrm{a}})\right] u(t - DT_{\mathrm{c}}) \tag{4}$$

$$V^{\mathrm{DC-}}_{\mathrm{sdrop}}(t) = \left[V_{\mathrm{I2}}(i_{\mathrm{a}})\right] u(t) - \left[V_{\mathrm{I2}}(i_{\mathrm{a}}) + V_{\mathrm{D1}}(i_{\mathrm{a}})\right] u(t - DT_{\mathrm{c}}). \tag{5}$$

B. Analytic Expression for Voltage Drop With Alternating Load Current

In most applications, alternating currents are applied to the machine. This necessitates an ac waveform representation, $V^{\mathrm{AC}}_{\mathrm{A}\to\mathrm{DCN}}$, to which there are two approaches. The first is representing $V^{\mathrm{AC}}_{\mathrm{A}\to\mathrm{DCN}}$ analytically as was done with $V^{\mathrm{DC}}_{\mathrm{A}\to\mathrm{DCN}}$. The second assumes that $V^{\mathrm{AC}}_{\mathrm{A}\to\mathrm{DCN}}$ is a succession of "$V^{\mathrm{DC}}_{\mathrm{A}\to\mathrm{DCN}}$-like" signals.

In [21], an analytic expression of a pulse train whose duty cycle is modulated with a sinusoid is developed using Bessel functions. This is applied to the sensor setup in this paper, resulting in (6) for a trailing edge signal with natural sampling. A microcontroller cannot calculate the spectrum quickly, as the spectrum calculation requires the sum of many Bessel functions to be accurate; thus, this approach is not taken

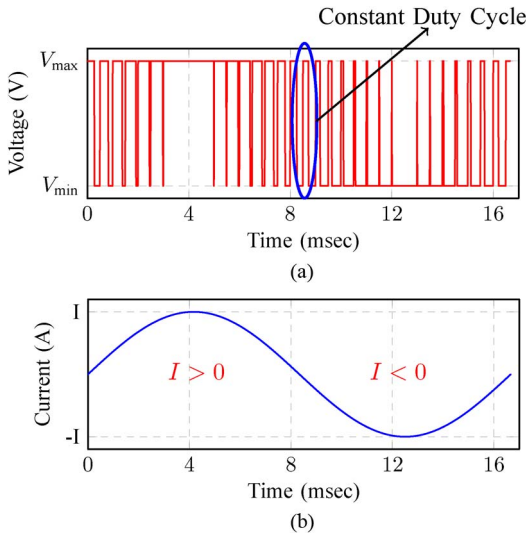

Fig. 5. $V_{\mathrm{A}\to\mathrm{DC}-}$ measurement for an ac waveform showing the relationship between current and the measured PWM voltage. The voltages are as follows: $(V_{\min}, V_{\max}) = (-V_{\mathrm{D2}}, V_{\mathrm{I1}})$ when current is positive, and $(V_{\min}, V_{\max}) = (-V_{\mathrm{D1}}, V_{\mathrm{I2}})$ when current is negative. (a) Simulated inverter phase voltage. (b) Simulated inverter phase current.

$$\begin{aligned} V^{\mathrm{AC}}_{\mathrm{A}\to\mathrm{DCN}}&(t, M, f_1, V_{\mathrm{DC}}, V_{\mathrm{I1}}, V_{\mathrm{I2}}, V_{\mathrm{D1}}, V_{\mathrm{D2}}, i_{\mathrm{a}}, f_{\mathrm{c}}) \\ &= \left\{\frac{1}{2}\left(\mathrm{sgn}(i_{\mathrm{a}}) + 1\right)\frac{V_{\mathrm{DC}} - V_{\mathrm{I1}} - V_{\mathrm{D2}}}{2} + \frac{1}{2}\left(-\mathrm{sgn}(i_{\mathrm{a}}) + 1\right)\frac{V_{\mathrm{I2}} - V_{\mathrm{D1}} - V_{\mathrm{DC}}}{2}\right\} \\ &\times\left\{M\sin(2\pi f_1 t) + \sum_{k=1}^{\infty}\frac{2}{k\pi}\left[1 - (-1)^k J_0(k\pi M)\right] \times \sin(2\pi k f_{\mathrm{c}} t) - \sum_{k=1}^{\infty}(-1)^k \sum_{n=1}^{\infty}\frac{J_{\mathrm{n}}(k\pi M)}{k\pi} \right. \\ &\left. \times\left[\sin(2\pi(kf_{\mathrm{c}} - nf_1)t) + (-1)^n \sin(2\pi(kf_{\mathrm{c}} + nf_1)t)\right]\right\} \\ &+ \frac{1}{2}\left(\mathrm{sgn}(i_{\mathrm{a}}) + 1\right)\frac{V_{\mathrm{DC}} - V_{\mathrm{I1}} - V_{\mathrm{D2}}}{2} + \frac{1}{2}\left(-\mathrm{sgn}(i_{\mathrm{a}}) + 1\right)\frac{V_{\mathrm{I2}} + V_{\mathrm{D1}} + V_{\mathrm{DC}}}{2}. \end{aligned} \tag{6}$$

The second approach approximates $V^{\mathrm{AC}}_{\mathrm{A}\to\mathrm{DCN}}$, as shown in Fig. 5(a), as many dc waveforms, like that in Fig. 4(c). Fig. 5(b) gives the corresponding current, and because this contains both positive and negative currents, all devices in that phase can be measured with this one test. Furthermore, as long as the amplitude of the current is high enough to saturate the semiconductors, the phase leg can be completely characterized. The ACPWM signal, a pulse train with time-varying duty cycle in Fig. 5(a), is viewed as a succession of constant duty cycle waveforms; one area of constant duty cycle is marked in Fig. 5(a). We can use (3) to model the voltage in the constant duty cycle area.

III. Methods Utilizing Direct Current

The representations for inverter semiconductor voltage drops are used to develop methods for inverter characterization. Direct load current is used to characterize the inverter devices. When a constant direct load current is applied, the semiconductor voltage drops for positive and negative currents are given by (4) and (5). Characterization methods are introduced first analytically and then are verified with simulations and experiments. There are two methods: one using the mean of V_{sdrop} and the other using its spectrum.

A. Method Utilizing the Voltage Mean

The mean method uses the mean of the square wave semiconductor voltage drop signal (μ_{x}) along with the duty cycle (D) with

$$\mu_{\mathrm{x}} = (1-D)(-V_{\mathrm{D2}}) + (D)(V_{\mathrm{I1}}). \tag{7}$$

To be able to solve for both unknowns in (7), another equation is required. This is accomplished by artificially increasing the duty cycle command in each phase. If the duty cycle applied to all phases is increased by the same amount, the voltage applied to the machine does not change. The measurement is taken once and then a second time by adding 5% to the duty cycle of each phase PWM command. With this, the nonlinearity equations at a given current can be found by equation set

$$\frac{D_2}{D_1}\mu_1 - \mu_2 = -V_{\mathrm{D2}}\left(\frac{D_2(1-D_1)}{D_1} - (1-D_2)\right)$$

$$V_{\mathrm{D2}} = \frac{-\frac{D_2}{D_1}\mu_1 + \mu_2}{\frac{D_2(1-D_1)}{D_1} - (1-D_2)}$$

$$V_{\mathrm{I1}} = \frac{\mu_1 + (1-D_1)V_{\mathrm{D2}}}{D_1}. \tag{8}$$

The mean method is first tested using a simulation of an inverter connected to an electric machine at standstill. A sampling frequency of 100 kHz and a switching frequency of 5 kHz, values typical in an industrial inverter, are used. The sampling frequency is sufficient to calculate up to the 10th switching harmonic, per the Nyquist criterion.

The inverter model used for simulations has the following parameters for each respective device: $V_{\mathrm{th,d}} = 1.2$ V, $V_{\mathrm{th,i}} = 1.3$ V, $R_{\mathrm{d}} = 4$ mΩ, and $R_{\mathrm{i}} = 6$ mΩ.

With any dc method, the current goes through one machine phase and returns through the other two with half the magnitude. To characterize over the entire operating range, only the maximum magnitude phase is used. By repeating these tests for both current directions in each phase, the voltage–current relationship for every device is found.

To test the performance of the proposed methods, data gathered with a high sampling rate, 2 MS/s, are used to estimate the semiconductor voltage drop. Verification is performed with the high sampling rate data by averaging all upper values of V_{sdrop}, defined when V_{sdrop} is greater than zero; for the bottom, this is done by averaging the values when V_{sdrop} is less than zero. The average of the upper values corresponds to the IGBT voltage; that of the lower ones corresponds to the diode voltage. This is termed the "high sampling frequency method."

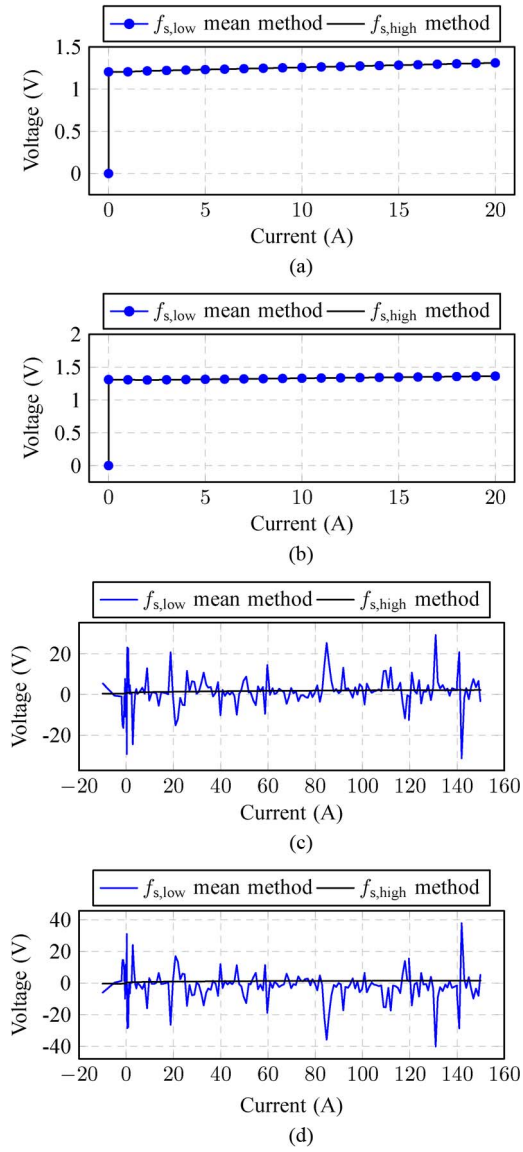

Fig. 6. Resulting simulation and experimental waveforms for voltage with the mean method. (a) Simulated voltage for an IGBT. (b) Simulated voltage for a diode. (c) Experimental voltage for an IGBT. (d) Experimental voltage for a diode.

The mean method is tested in simulation for one phase, at all currents from 0 to 20 A in 1-A steps. The method performs well in simulation as seen in Fig. 6(a) and (b), matching the high sampling frequency method results.

The mean method is then experimentally verified. The experimental setup consists of a three-phase induction machine with a current rating of 200 A connected to a 1200-V SEMIKRON SKiiP 2 inverter with a current rating of 300 A. A dSPACE system controls the inverter and is programmed to allow for either ac or dc control, and it has all phase current sensors as well as a dc-link voltage sensor.

An HBM GEN2i data acquisition system is used to sense all currents and voltages as shown in Fig. 2, including phase-to-negative dc-link voltage sensors. The GEN2i system samples

at 2 MS/s for high-frequency verification, but the signal is downsampled to 100 kS/s to match a typical DSP sampling rate.

A range of positive direct currents were applied to phase A of the machine from 0 to 150 A with a step size of 1 A. Calculating the square wave mean is very susceptible to noise, which is seen in the resulting nonlinearity waveforms in Fig. 6(c) and (d). The high-order switching harmonics cannot be filtered to reduce the noise; doing so would produce a signal which is no longer a square wave and would not be compatible with (8).

B. Method Utilizing the Waveform Spectrum

The second method, termed the "spectral method," is proposed. Given that the mean method is noise prone, a more robust method is sought, using the same conditions of the mean method. The Fourier spectrum of the PWM voltage was investigated to find the voltage drops since, if no aliasing occurs, the low frequency spectrum can be determined without high-frequency noise. The measured semiconductor voltage drop in (9) is used to derive the analytic expression of the DFT in (10).

N_p in (10) represents the number of samples which lie in the positive portion of the PWM signal; this must be determined to allow for the accurate calculation of the device parameters. Rather than determining the value from the sampled signal, it is more useful to calculate the value. The value can be determined using the PWM frequency, duty cycle, and the sampling rate, and care must be taken to take into account the phase delay in sampling

$$\begin{aligned} x[n] &= V_{\mathrm{I1}}u[n] - (V_{\mathrm{I1}} + V_{\mathrm{D2}})u\left[n - (DN+1)\right]) \\ &= x[n+N] \end{aligned} \tag{9}$$

$$C_0 = \frac{(V_{\mathrm{D2}} + V_{\mathrm{I1}})N_\mathrm{p}}{N} - V_{\mathrm{D2}} \tag{10}$$

$$|C_\mathrm{k}| = \frac{V_{\mathrm{D2}} + V_{\mathrm{I1}}}{N} \frac{\sin\left(\frac{\pi k N_\mathrm{p}}{N}\right)}{\sin\left(\frac{\pi k}{N}\right)}. \tag{11}$$

The relationship between the device characteristics and harmonics is defined by this analytic representation of the DFT of V_{sdrop}. Once again, there are two unknowns with one equation. In this case, two equations are found by selecting two harmonics and their respective equations: the first and dc harmonics. The device characteristics can be computed with the following: these two equations, the number of samples, the duty cycle, and the dc and first harmonic values. For this method, the FFT must be computed by the inverter's DSP or microcontroller at the dc and fundamental switching frequency (5 kHz). The resulting characteristics of IGBT1 and diode2 are found with (12) and given in Fig. 7(a) and (b) from simulations and Fig. 7(c) and (d) from experiments. This method can effectively estimate the nonlinearity for each device with minimal loss of precision due to noise

$$V_{\mathrm{D2}} = N_\mathrm{p}\mathrm{FFT}(1)\frac{\sin\left(\frac{\pi}{N}\right)}{\sin\left(\frac{N_\mathrm{p}\pi}{N}\right)} - \mathrm{FFT}(0)$$

$$V_{\mathrm{I1}} = N\mathrm{FFT}(1)\frac{\sin\left(\frac{\pi}{N}\right)}{\sin\left(\frac{N_\mathrm{p}\pi}{N}\right)} - V_{\mathrm{D2}}. \tag{12}$$

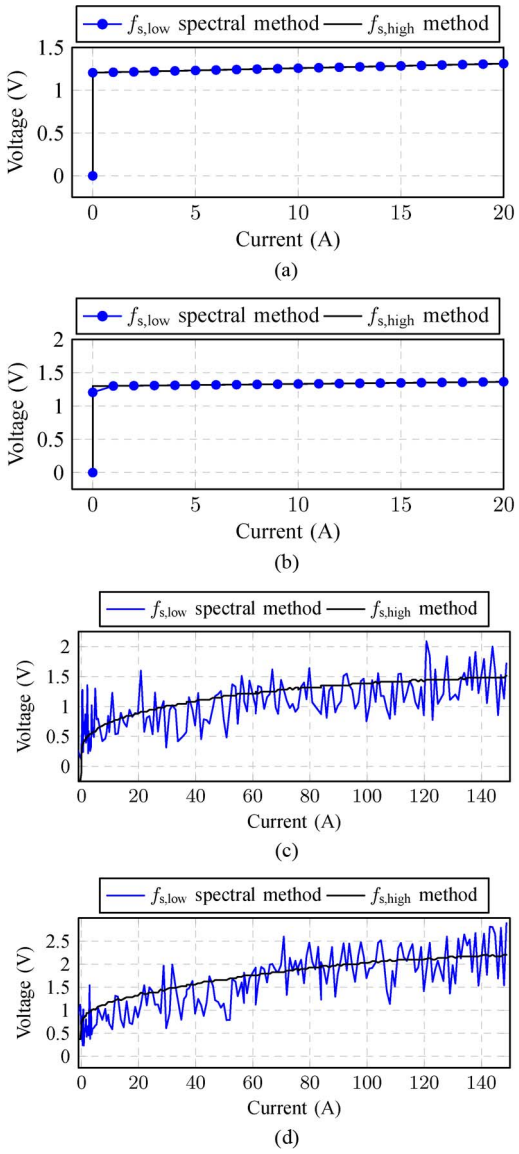

Fig. 7. Resulting simulation and experimental waveforms for voltage with the spectral method. (a) Simulated voltage for an IGBT. (b) Simulated voltage for a diode. (c) Experimental voltage for an IGBT. (d) Experimental voltage for a diode.

IV. Methods Utilizing Alternating Current

Inverter characterization is accomplished by using alternating current in two ways. The first method, termed the "algorithm method," uses measurements of the measured voltage signal and a simple algorithm to determine the device characteristics. The second approach uses a variation of the spectral method from Section III-B using the knowledge that the duty cycle is constant in a local area. To test the performance of the proposed ac methods, the high sampling rate data are used with the algorithm method, and the result is filtered.

A. Characterization With Developed Algorithm

An "algorithm method" is developed to use the measured ac voltage with respect to the current to find the voltage–current relationship for each device. In Fig. 5(a), the voltage of phase A

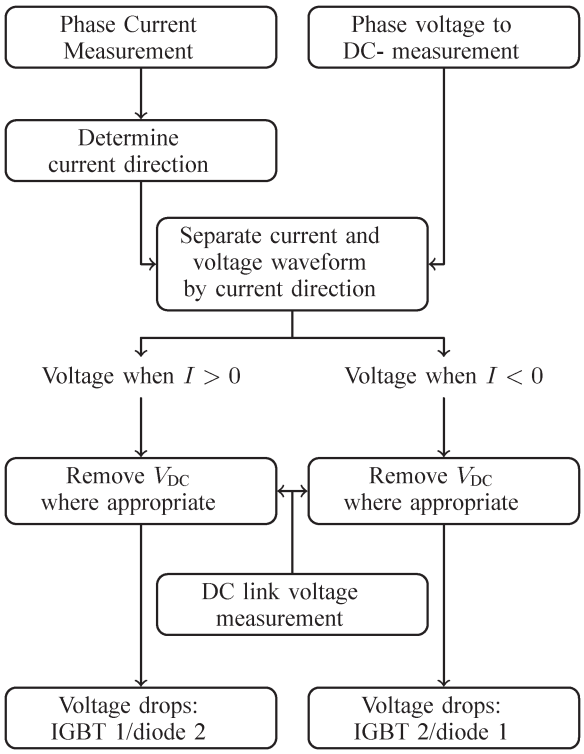

Fig. 8. Characterization method used to determine the voltage and current relationship of inverter devices.

is shown with respect to the current in Fig. 5(b). This waveform contains voltage data for both directions of current, so it is possible to characterize the top and bottom IGBTs and diodes, as well as their respective freewheeling diodes.

If the current values are associated with their respective voltages, a model can be constructed for each device. In implementation, only integer-valued currents are stored, by rounding all current readings to the nearest integer. Voltage readings taken at 1.5 A→2.49 A are averaged and stored for the 2-A point; this reduces the number of points in the model. Thus, the model will consist of two vectors: $(0\ \mathrm{A},\ 1\ \mathrm{A}, \ldots, I_{\max}\ \mathrm{A})$ and $(V_{0\,\mathrm{A}}\ \mathrm{V},\ V_{1\,\mathrm{A}}\ \mathrm{V}, \ldots, V_{I_{\max}\ \mathrm{A}}\ \mathrm{V})$.

Fig. 8 shows the algorithm to find the appropriate voltage with respect to current. The inverter can be characterized by one ac point, if a sinusoidal current is applied which has a peak value within the saturation area of the IGBT and diode, as every intermediate current is also contained in that data.

The same setup as the dc methods is used, but with an ac of 150 A_{peak} applied. The results in Figs. 9 and 10 match well to that of the verification method.

B. Method Using DC Approximation With STFT

A method using the spectrum of the voltage is proposed for use with ac current; this is termed the "AC spectral method." The problem with applying the spectral method directly to the ac signal is that this method calculates the FFT for the entire time span; in the dc case, this is a stationary signal and thus appropriate. The harmonics of a stationary signal do not change in time; with the varying duty cycle waveform that results when measuring the voltage while alternating current is applied,

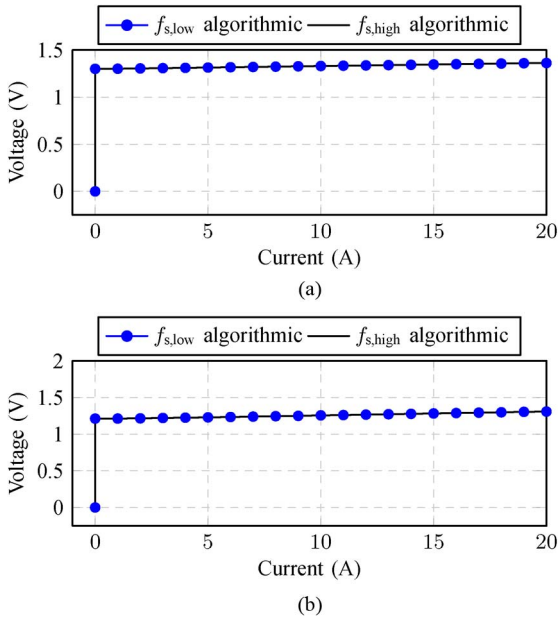

Fig. 9. Simulation results of nonlinearity voltage drop with algorithm method. (a) Simulated voltage for an IGBT. (b) Simulated voltage for a diode.

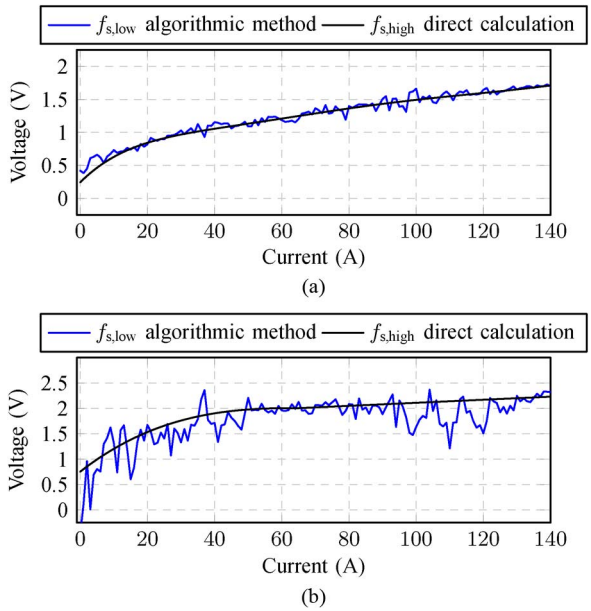

Fig. 10. Experimental results of nonlinearity voltage drop with algorithm method. (a) Experimental voltage for an IGBT. (b) Experimental voltage for a diode.

this is not the case. It is possible to calculate the FFT of the entire signal, but the voltage–current relationship is lost, as the harmonics correspond to multiple currents.

Taking the FFT in a localized region, like that circled in Fig. 5(a), would remedy this if the FFT is calculated for a local dc-like area with roughly constant current. This is possible with the STFT shown in (13) [20]

$$\mathrm{STFT}(t, f) = \int h(t-\tau)s(\tau)e^{-j2\pi f\tau}d\tau. \qquad (13)$$

The simplest STFT window is the rectangular window, with a magnitude of one for all samples within the window and zero

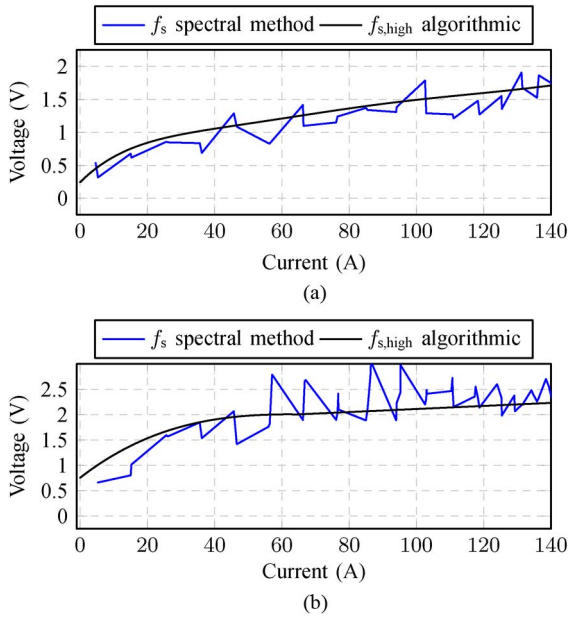

Fig. 11. Experimental results of voltage drop spectrum extraction for ac using STFT. (a) Experimental voltage for an IGBT. (b) Experimental voltage for a diode.

otherwise. The analytic derivation of the DFT is shift invariant, as is seen in (16)–(18), where the DFT of two shift instances given by (14) and (15) is calculated. The magnitude of the spectrum ends up being the same since the $x[n]$ waveform, the product of the window and the PWM waveform, is one over the nonzero indices

$$x[n] = \begin{cases} 1, & \text{if } n = 0, 1, 2, 3, 4 \\ 0, & \text{otherwise} \end{cases} \tag{14}$$

$$x[n-1] = \begin{cases} 1, & \text{if } n = 1, 2, 3, 4, 5 \\ 0, & \text{otherwise} \end{cases} \tag{15}$$

$$C_k = \sum_{n=0}^{N-1} x[n] \frac{e^{\frac{-jkn2\pi}{N}}}{N} = \sum_{n=0}^{N-1} x[n-1] \frac{e^{\frac{-jkn2\pi}{N}}}{N} \tag{16}$$

$$C_k = \sum_{n=0}^{4} \frac{e^{\frac{-jkn2\pi}{N}}}{N} = \sum_{n=1}^{5} \frac{e^{\frac{-jkn2\pi}{N}}}{N} \tag{17}$$

$$|C_k| = \frac{1}{N} \frac{\sin\left(kN_{\mathrm{p}} \frac{\pi}{N}\right)}{\sin\left(k \frac{\pi}{N}\right)} = \frac{1}{N} \frac{\sin\left(kN_{\mathrm{p}} \frac{\pi}{N}\right)}{\sin\left(k \frac{\pi}{N}\right)}. \tag{18}$$

When the values of the window are not constant and depend on n, $x[n]$, the analytic derivation of the DFT changes depending on where the waveform is sampled. If the PWM waveform is shifted and this is multiplied by the window function, the result changes; this would require the derivation of a new analytic DFT function. This is the drawback to using the default window in the *spectrogram* function, the Hamming window. If the sampling shift changes, a new set of equations must be used to calculate the device characteristics. For these reasons, the rectangular window is chosen for characterization.

The MATLAB [22] function *spectrogram* is used with a rectangular *window* size five times the number of samples per period, *overlap* is set to half of the PWM period, and *nfft* is set to the *window* size.

The DC method equations in (12) are used with the harmonic information found using the STFT to find the characteristics in Fig. 11(a) and (b). These figures show the results for the phase A positive current quantities, IGBT1 and diode2, although all devices can be characterized using this method.

V. Conclusion

In this paper, a novel inverter characterization procedure was investigated. The benefit of this method lies in its ability to identify individual device parameters as they vary during operation, an important goal in monitoring the condition of all devices. The spectral method accurately characterizes the inverter; the mean method is too noise prone to do this. With the spectral method and the calculation of the FFT, the nonlinearities of interest are found. This is successfully extended to the alternating current case by way of the STFT. With the simulated and the experimental work, these methods prove useful for the monitoring of inverter nonlinearities with both direct and alternating currents.

References

[1] J. Holtz and J. Quan, "Sensorless vector control of induction motors at very low speed using a nonlinear inverter model and parameter identification," *IEEE Trans. Ind. Appl.*, vol. 38, no. 4, pp. 1087–1095, Jul./Aug. 2002.
[2] R. Raute *et al.*, "Analysis and compensation of inverter nonlinearity effect on a sensorless PMSM drive at very low and zero speed operation," *IEEE Trans. Ind. Electron.*, vol. 57, no. 12, pp. 4065–4074, Dec. 2010.
[3] G. Pellegrino, P. Guglielmi, E. Armando, and R. Bojoi, "Self-commissioning algorithm for inverter nonlinearity compensation in sensorless induction motor drives," *IEEE Trans. Ind. Appl.*, vol. 46, no. 4, pp. 1416–1424, Jul./Aug. 2010.
[4] K. Liu and Z. Zhu, "Online estimation of the rotor flux linkage and voltage-source inverter nonlinearity in permanent magnet synchronous machine drives," *IEEE Trans. Power Electron.*, vol. 29, no. 1, pp. 418–427, Jan. 2014.
[5] A. Weber and G. Steiner, "An accurate identification and compensation method for nonlinear inverter characteristics for ac motor drives," in *Proc. IEEE I2MTC*, 2012, pp. 821–826.
[6] D. Salt *et al.*, "Compensation of inverter nonlinear distortion effects for signal-injection-based sensorless control," *IEEE Trans. Ind. Appl.*, vol. 47, no. 5, pp. 2084–2092, Sep./Oct. 2011.
[7] J.-W. Choi and S.-K. Sul, "Inverter output voltage synthesis using novel dead time compensation," *IEEE Trans. Power Electron.*, vol. 11, no. 2, pp. 221–227, Mar. 1996.
[8] Y. Murai, T. Watanabe, and H. Iwasaki, "Waveform distortion and correction circuit for PWM inverters with switching lag-times," *IEEE Trans. Ind. Appl.*, vol. IA-23, no. 5, pp. 881–886, Sep. 1987.
[9] S.-G. Jeong and M.-H. Park, "The analysis and compensation of deadtime effects in PWM inverters," *IEEE Trans. Ind. Electron.*, vol. 38, no. 2, pp. 108–114, Apr. 1991.
[10] S. Yang *et al.*, "Condition monitoring for device reliability in power electronic converters: A review," *IEEE Trans. Power Electron.*, vol. 25, no. 11, pp. 2734–2752, Nov. 2010.
[11] Y. Song and B. Wang, "Survey on reliability of power electronic systems," *IEEE Trans. Power Electron.*, vol. 28, no. 1, pp. 591–604, Jan. 2013.
[12] Y. Xiong *et al.*, "Prognostic and warning system for power-electronic modules in electric, hybrid electric, and fuel-cell vehicles," *IEEE Trans. Ind. Electron.*, vol. 55, no. 6, pp. 2268–2276, Jun. 2008.
[13] D. Diallo, M. Benbouzid, D. Hamad, and X. Pierre, "Fault detection and diagnosis in an induction machine drive: A pattern recognition approach based on concordia stator mean current vector," *IEEE Trans. Energy Convers.*, vol. 20, no. 3, pp. 512–519, Sep. 2005.
[14] D. Xiang *et al.*, "Condition monitoring power module solder fatigue using inverter harmonic identification," *IEEE Trans. Power Electron.*, vol. 27, no. 1, pp. 235–247, Jan. 2012.

[15] J. Estima and A. J. Marques Cardoso, "A new algorithm for real-time multiple open-circuit fault diagnosis in voltage-fed PWM motor drives by the reference current errors," *IEEE Trans. Ind. Electron.*, vol. 60, no. 8, pp. 3496–3505, Aug. 2013.
[16] J. Lehmann, M. Netzel, R. Herzer, and S. Pawel, "Method for electrical detection of bond wire lift-off for power semiconductors," in *Proc. 15th IEEE ISPSD ICs*, 2003, pp. 333–336.
[17] K. Smith, L. Ran, and J. Penman, "Real-time detection of intermittent misfiring in a voltage-fed PWM inverter induction-motor drive," *IEEE Trans. Ind. Electron.*, vol. 44, no. 4, pp. 468–476, Aug. 1997.
[18] Q.-T. An, L.-Z. Sun, K. Zhao, and L. Sun, "Switching function model based fast-diagnostic method of open-switch faults in inverters without sensors," *IEEE Trans. Power Electron.*, vol. 26, no. 1, pp. 119–126, Jan. 2011.
[19] I. R. Bojoi, E. Armando, G. Pellegrino, and S. G. Rosu, "Self commissioning of inverter nonlinear effects in ac drives," in *Proc. IEEE Int. ENERGYCON Exhib.*, 2012, pp. 213–218.
[20] W. Zanardelli, E. Strangas, and S. Aviyente, "Identification of intermittent electrical and mechanical faults in permanent-magnet ac drives based on time-frequency analysis," *IEEE Trans. Ind. Appl.*, vol. 43, no. 4, pp. 971–980, Jul./Aug. 2007.
[21] Z. Song and D. V. Sarwate, "The frequency spectrum of pulse width modulated signals," *Signal Process.*, vol. 83, no. 10, pp. 2227–2258, Oct. 2003.
[22] *MATLAB*, The MathWorks Inc., Natick, MA, USA, 2010.

Andrew S. Babel (S'12) received the B.S. and M.S. degrees in electrical engineering from Michigan State University, East Lansing, MI, USA, in 2009 and 2012, respectively, where he is currently working toward the Ph.D. degree in the Electrical Machines and Drives Laboratory.

From March through September 2013, he was a Visiting Researcher at Graz University of Technology, Graz, Austria, on the Marshall Plan Foundation Scholarship. His research interests include condition monitoring, machine design, and the control of electrical machines and power electronics.

Annette Muetze (S'03–M'04–SM'09) received the Dipl.Ing. degree in electrical engineering from Darmstadt University of Technology, Darmstadt, Germany, in 1999, the General Eng. degree from the Ecole Centrale de Lyon, Ecully, France, in 1999, and the Dr. Ing. degree in electrical engineering from Darmstadt University of Technology in 2004.

She is currently a Full Professor at Graz University of Technology, Graz, Austria, where she heads the Electric Drives and Machines Institute. She was an Assistant Professor in the Electrical and Computer Engineering Department, University of Wisconsin–Madison, Madison, WI, USA, and an Associate Professor with the School of Engineering, University of Warwick, Coventry, U.K.

Roland R. Seebacher was born in Lienz/Osttirol, Austria, in 1961. He received the M.S. and Ph.D. degrees in electrical engineering from Graz University of Technology, Graz, Austria, in 1991 and 1996, respectively.

He is currently an Assistant Professor with the Institute of Electrical Drives and Machines, Graz University of Technology. His research interests are in the area of modeling and control of electric machines and drives.

Klaus Krischan received the Dipl.Ing. degree and the Dr. degree in electrical engineering from Graz University of Technology, Graz, Austria, in 1990 and 1995, respectively.

He joined the Electric Drives and Machines Institute (then known as the Institute for Electro Magnetic Energy Conversion) at Graz University of Technology as a student assistant in 1989, where he currently is an Assistant Professor. His main research and teaching activities deal with switch-mode power conversion in combination with electrical drives.

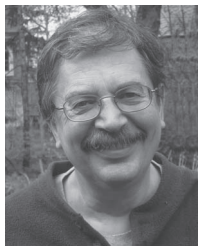

Elias G. Strangas (M'80) received the Dipl.Eng. degree in electrical engineering from the National Technical University of Greece, Athens, Greece, and the Ph.D. degree from the University of Pittsburgh. Pittsburgh, PA, USA, in 1980.

He was with Schneider Electric Athens from 1981 to 1983 and the University of Missouri–Rolla from 1983 to 1986. Since 1986, he has been with the Department of Electrical and Computer Engineering, Michigan State University, East Lansing, MI, USA, where he heads the Machines and Drives Laboratory. His research interests include the design and control of electrical machines and drives and the failure prognosis and mitigation of electrical drives.